

Earth and Space Science



RESEARCH ARTICLE

10.1029/2019EA000968

Key Points:

- This work investigates subsurface radar reflectors in the Central Elysium Planitia region based on SHallow RADar (SHARAD) data and posits an interpretation as to their formation
- Buried channels in the Cerberus Plain appear to be connected to Marte Vallis, and may also be connected to Athabasca Valles
- Depths of exposed layers in a terraced crater are measured. The depths appear to correspond to the depth of radar layers, and this retrieval favors an interpretation of shallow buried water ice or composites with other dry low-density materials

Supporting Information:

- Supporting Information S1
- Data Set S1

Correspondence to:

S. Xiong and J.-P. Muller,
siting.xiong.14@alumni.ucl.ac.uk;
j.muller@ucl.ac.uk

Citation:

Xiong, S., Tao, Y., Persaud, D. M., Campbell, J. D., Putri, A. R. D., & Muller, J. P. (2020). Subsurface reflectors detected by SHARAD reveal stratigraphy and buried channels over central Elysium Planitia, Mars. *Earth and Space Science*, 7, e2019EA000968. <https://doi.org/10.1029/2019EA000968>

Received 25 OCT 2019
 Accepted 24 OCT 2020
 Corrected 8 MAR 2021

This article was corrected on 8 MAR 2021. See the end of the full text for details.

© 2020 The Authors.

This is an open access article under the terms of the [Creative Commons Attribution-NonCommercial-NoDerivs License](#), which permits use and distribution in any medium, provided the original work is properly cited, the use is non-commercial and no modifications or adaptations are made.

Subsurface Reflectors Detected by SHARAD Reveal Stratigraphy and Buried Channels Over Central Elysium Planitia, Mars

Siting Xiong¹ , Yu Tao¹ , Divya M. Persaud¹ , Jacqueline D. Campbell¹ , Alfiah Rizky Diana Putri¹ , and Jan-Peter Muller¹ 

¹Imaging Group, Mullard Space Science Laboratory, Department of Space and Climate Physics, University College London, Dorking, Surrey, UK

Abstract The Central Elysium Planitia (CEP) is one of the youngest geological units on Mars and displays evidence of volcanic and fluvial activities on the surface. The origin of the CEP material has long been debated with a range of hypotheses from purely fluvial to solely volcanic origins. This study presents a comprehensive investigation of SHallow RADar (SHARAD) data to reveal subsurface radar reflectors over the CEP region. Distribution of the detected radar reflectors show possible connections between the CEP and outflow channels, such as Athabasca Valles and Marte Vallis. Analysis of the radar reflectors in the CEP region show six subsurface layers implying multiple depositional and erosional episodes. One detected subsurface layer is found to correspond to the upper exposed layers of one terraced crater. By measuring the depth accurately of these exposed layers in the derived HiRISE (High Resolution Imaging Scientific Experiment) and CTX (Context Camera) DTMs (Digital Terrain Models) and inverting the dielectric constant combining the layers in radargrams, an interpretation that the filling material contains water ice is favored.

1. Introduction

The Cerberus plains, is a broad low-lying plain in the central part of Elysium Planitia (CEP) on Mars extending from about 140°E to 185°E and from 5°S to 10°N (Cassanelli & Head, 2018; Plescia, 1990, 2003; Vaucher et al., 2009). The surface of this region is separated from one extremely young unit dating from ~250 to ~2 Mya in the late Amazonian period, while the other older unit dates from about ~500 Mya (Tanaka et al., 2014; Vaucher et al., 2009). Four outflow channel systems have been identified in this region; these are Athabasca Valles in the west, Grjotá Valles in the north, and Rahway Valles and Marte Vallis in the north-east (Burr et al., 2002; Cassanelli & Head, 2018; Plescia, 2003; Tanaka et al., 2014). A series of extensional fissures, the west-northwest-trending Cerberus Fossae, extend over a total length of more than 1,200 km in this region, which has been proposed as the source of these channel systems (Head & Marchant, 2003; Jaeger et al., 2010; Plescia, 2003). The interior morphology of Cerberus Fossae consists of a steep, layered upper slope and a gentler lower slope, which are presumably composed of exposed bedrock and talus, respectively (Plescia, 2003).

Various landforms observed in this region have resulted in several hypotheses as to the origin of the Cerberus plains material, from a purely aqueous origin to a purely volcanic one. For example, Athabasca Valles is thought to have been carved by a high-discharge flood of water based on streamlined islands, notches on the sides of the breach hanging valleys and a low number of tributaries, while other authors have argued that this channel might be carved by fluid lava, which is supported by fissure vents (Plescia, 2000), long lava flows (Berman & Hartmann, 2002; Lanagan, 2004), and shield volcanoes (Plescia, 1990, 2003). There is evidence for numerous constructional and erosional landforms, such as relic waterfalls, down-cut erosional channels, streamlined islands within the channels, notches on the sides of the breach hanging valleys, and eroded topographic obstacles (Durrant et al., 2017; Kossacki et al., 2006; Murray et al., 2005). These suggest that fluvial events carved the current landforms in the Athabasca Valles. Murray et al. (2005) proposed that a frozen body of water with surface pack-ice might explain fluvial landforms including lobate scarps, troughs, sinuous ridges, and platy-ridged terrains in the Athabasca basin. On the other hand, volcanic landforms, such as linear fissure vents (Plescia, 2000), long lava flows (Berman & Hartmann, 2002;

Lanagan, 2004), and shield volcanoes (Plescia, 1990, 2003), are also observed in this region, possibly suggesting a volcanic origin for the outflow channel systems (Jaeger et al., 2007, 2008). A low-viscosity lava flow model of a lower eruption rate (1.4×10^{-2} to 1.8×10^{-2} m³/s) and long, inactive periods are also proposed to explain the volcanic landforms (Vaucher et al., 2009). As more observations become available in higher resolution surface imagery from Mars Orbiter Camera (MOC, Malin et al., 2010), Context Camera (CTX, Malin et al., 2007) and High Resolution Imaging Science Experiment (HiRISE, McEwen et al., 2007), discussion about the formation of landforms in this region is no longer limited to a single fluvial or a volcanic event. More complex and multiple event interactions have more recently been proposed to explain these observations. For instance, it was proposed that the Martian outflow channel systems, including these four channel systems, were carved out by water either released by groundwater burst (Balme et al., 2010; Burr et al., 2004; Carr, 1996; Clifford, 1993; Harrison & Grimm, 2005; Head & Marchant, 2003) or lava-ice interactions (Cassanelli & Head, 2018). Voigt and Hamilton (2018) mapped 19 morphologically distinct regions using facies over the eastern Elysium Planitia, including Eastern Cerberus Fossae, Rahway Valles and Marte Vallis, showing this region was resurfaced by at least two volcanic flows with much younger ages of 20 and 8.8 Ma, as there is an erosional unconformity located between two youngest lava flow units in Marte Vallis. They infer that the outflow channels were carved out by catastrophic fluvial events and emplaced by more recent flood lava (Voigt & Hamilton, 2018). From several threads of clues, there appears to be a consensus that aqueous floods had carved the outflow channels which were later emplaced by lava flows (Keszthelyi et al., 2017; G. A. Morgan et al., 2013). However, the timing and the magnitude of the postulated aqueous floods, and whether they immediately preceded the lava flows or were much earlier is unclear.

Interpretation of sedimentary and erosional history, especially the timings of aqueous and igneous floods of this region has been limited to orbital imagery of the surface until the availability of subsurface detection achieved by SHARAD onboard Mars Reconnaissance Orbiter (MRO, Seu et al., 2004), which is an orbital sounding radar instruments to investigate the upper crust of Mars. This instrument transmits pulsed radar signals at nadir and receives echoes returning from the surface and subsurface Mars. These echoes can be processed to generate profile images whose vertical resolution is 15 m in vacuum, and approximately 8 m in water ice (Stuurman et al., 2016). The spatial along-track resolution is between 0.3–1 km and the across-track resolution between 3–6 km (Seu et al., 2004; Stuurman et al., 2016). SHARAD provides us with a way to image the upper part of the Martian crust down to at most ~5 km (Seu et al., 2004) and to infer its material composition. It has been used to detect subsurface water ice in the South polar layered deposits, Medusae Fossae, etc. (Campbell & Morgan, 2018). The objective of this study is to investigate SHARAD radar reflectors over the wider CEP region, to reveal subsurface interfaces and to interpret the depositional and erosional history with the assistance of surface imagery and derived DTMs from HiRISE and CTX. In the following sections, the study region is described in more detail followed by display of results of detected radar reflectors in the study region, and discussion of the formation of subsurface layering.

2. Materials and Methods

2.1. Study Area and Geological Context

Elysium Planitia is characterized as one of the youngest geologic units on Mars and is located southeast of the Elysium Mons as shown in Figure 1. Lying at the dichotomy boundary between the low northern circumpolar plains and the densely cratered southern hemisphere, it is bounded by Amazonis Planitia to the northeast and Medusae Fossae to the southeast. This region is dominated by the surficial geologic material of Late to Middle Amazonian Cerberus Fossae 2 (AEC₂ or ACo) unit, which has a distinctively smooth surface as compared to the Late Amazonian Cerberus Fossae 3 (AEC₃ or ACy) unit (Tanaka et al., 2014; Vaucher et al., 2009). Vaucher et al. (2009) have estimated the surface age of AEC₃ to be very young at only $16\text{--}25 \pm 2$ Ma.

The study region is selected in the central part of Elysium Planitia, extending from 10°S to 20°N and from 140°W to 190°E, as indicated by the black box shown in Figure 1. The AEC₃ unit occupies the main part of the study region, which is a low lying flat plain of extremely low regional slope (10 m over a 500 km distance, Balme et al., 2010). This flat plain is characterized by meter-scale features, which appear smooth in the SHARAD data. The flat plain mainly consists of the Cerberus Plain, Rahway Valles, and Marte Vallis.

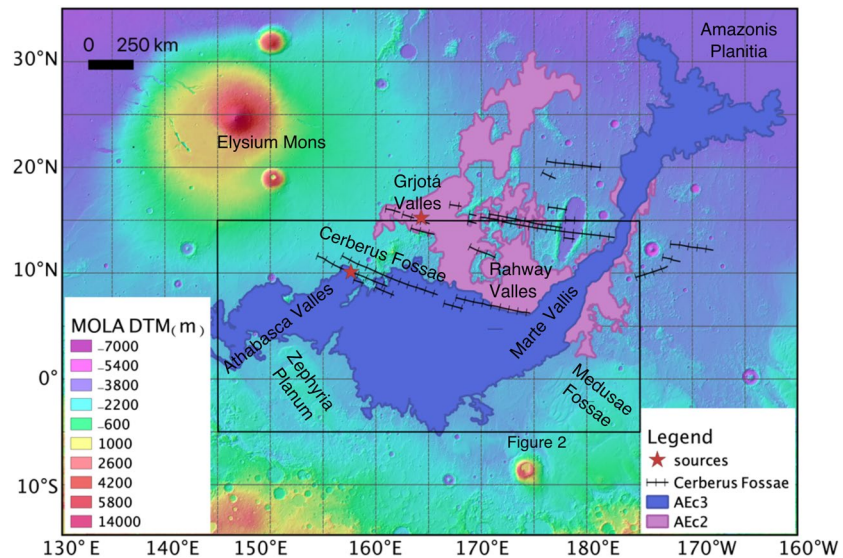


Figure 1. Central Elysium Planitia region. The black box indicates the study area extent, and detected radar reflectors in this region are shown in Figure 2. The stars show the source of outflow channel of Athabasca Valles and Grjotá Valles.

The surrounding areas have a higher topography and their surface units are interpreted to be older. To the south, there is a Cerberus Fossae 1 (AEC₁) unit, which is interpreted to be a part of the Medusae Fossae unit (Voigt & Hamilton, 2018). To the north, it is mainly composed of the Noachian-age Nepenthes Mensae unit.

Athabasca Valles is located west of the Cerberus plain and is postulated to be sourced from a western fissure of Cerberus Fossae. Grjotá Valles is located north of the Cerberus plain and is interpreted to be sourced from a northern fissure of Cerberus Fossae. The sources of the two channels is indicated by a red star shown in Figure 1. Marte Vallis is inferred to be formed during the Amazonian Period, and its age is ≤ 200 Ma (Voigt & Hamilton, 2018). The source of floodwater that carved Marte Vallis may have originated from an eastern fissure of Cerberus Fossae, which has since been buried by lava flows and is 180 km southeast to the visible southeast end of the fissure and the channel depth which was estimated to be at least 80 m based on SHARAD data (Morgan et al., 2013). Marte Vallis appears to flow from this source to Amazonis Planitia. Their planar and stratigraphic distributions led to the conclusion that later lava floods filled in the eroded channels carved out by several large fluvial floods (Morgan et al., 2013). Compared to Marte Vallis, channels in Rahway Valles have a higher-order tributary system (Ramsdale et al., 2015), implying lower energy during its formation. Therefore, it is interpreted to be non-catastrophic fluvial activity that formed the channels (Plescia, 2003).

Several groups have investigated the SHARAD data of Athabasca Valles, as well as the central part of the Cerberus plain and Marte Vallis (Alberti et al., 2012; Morgan et al., 2013, 2015). Previously published results show few subsurface radar reflectors were observed in SHARAD radargrams over Athabasca Valles (Alberti et al., 2012; Orosei et al., 2007), while abundant subsurface reflectors were revealed over Marte Vallis (Morgan et al., 2013), and central Cerberus plain (Morgan et al., 2015). In this study, we investigate SHARAD data over a wider area combining reports from several previous studies, including east of the Athabasca basin, the Main Cerberus basin and Marte Vallis. This provides an opportunity to investigate possible connections between CEP and the surrounding four outflow channels.

2.2. Data and Methodology

The primary dataset used in this study is SHARAD data released by the SHARAD team at the NASA Jet Propulsion Laboratory (JPL), USA. Over the study area, 877 SHARAD radargrams in total were collected and manually digitized to generate depth maps of subsurface radar reflectors. To try to accelerate this process,

we also tested an automated layer extraction method, SHARAD3d proposed by Xiong and Muller (2019). A comparison between the manual and automated delineation can be seen in the [supporting information](#). On the one hand, the automated method, SAHARAD3d is much more efficient than manual digitization, with the time taken being a factor of about three times less, on the other hand, the detected reflectors are less continuous than the ones derived by manual digitization. Table S1 in the [supporting information](#) compares the number of SHARAD radargrams containing subsurface detections and the time saving using manual compared with automated methods. In the following description, we use product IDs of SHARAD radargrams which consist of four to five digits for identifying orbit and the last two digits for identifying the Operation Sequence Tableline (OST, Slavney and Orosei, 2007).

Apart from radar data, higher resolution surface images, such as HiRISE (25 cm) and CTX (6 m) data, were analyzed to assist with the interpretation. One HiRISE stereo-pair (ESP_043815_1840-ESP_044514_1840) and one CTX stereo-pair (F22_044514_1831_XN_03N195W and G02_018853_1837_XN_03N195W) were found in this area covering a terraced crater. These stereo-pairs were processed by applying the CASP-GO processing chain (Tao et al., 2018). Finally, one HiRISE DTM and one CTX DTM were derived over the terraced crater, and all were co-aligned with HRSC (High Resolution Stereo Camera on board ESA Mars Express) DTM using the flat area surrounding the crater. Mars Global Surveyor (MGS) Mars Orbiter Laser Altimeter (MOLA) Mission Experiment Gridded Data Records (MEGDRs) are used as a background image in this study and for analyzing elevation when it is necessary due to the lack of any wide area coverage by CTX or HiRISE stereo data being available.

3. Results

3.1. Connection of Buried Channels (Distribution of Radar Reflectors)

The time delay of detected radar reflectors is converted to depth below the surface assuming a single dielectric constant, 3.14 of water ice (Bramson et al., 2015; Stuurman et al., 2016) and the results are shown in Figure 2. The dielectric constant of most material on Mars is usually assumed to be above 3.0 apart from CO₂ ice where it is slightly lower than this (Stuurman et al., 2016). For instance, the dielectric constant of lava is about 8–10. In this study, we use a single value of 3.14 to convert time delays of radar reflectors to depths. Therefore, the depth maps represent a lower boundary of the depth. If the surface material has a higher dielectric constant, the detected radar reflectors should be much shallower. In Figure 2, flow directions in this region are postulated based on a manual interpretation and are displayed using red arrows (Tanaka et al., 2014). The black straight lines in Figure 2 indicate several selected radargrams with their reference numbers which are shown in Figure 3.

As shown in Figure 2, only a small number of reflectors are detected in the distal parts of Athabasca Valles, north of Zephyria Planum, in accordance with the results presented by Orosei et al. (2007). The radar stratigraphy appears to be related to the surficial unit type. For instance, Athabasca Valles is mainly occupied by younger units (AEC₂), and only one layer can be observed in SHARAD data as observed as L2 and red arrows in Figures 3a and 3b, respectively. By comparison, in Marte Vallis, there is an area occupied by the younger AEC₂ unit and only one single layer is detected as indicated by L3 in Figure 3f, which appears to be the same as the R3 layer detected by Morgan et al. (2013). However, in the central Cerberus plain, several layers can be observed as indicated by white arrows in Figure 3c and by L1–L6 in Figure 3d. This region is not occupied by a purely younger unit, but features a complex geomorphology and a higher density of craters, indicating remnants of older units. In comparison, in Rahway Valles, two layers (L1 and L2 in Figure 3f) can be observed while this region is occupied by the older AEC₂ unit.

In the Cerberus plain, radar reflectors are mainly detected under the central area. Spatially, most of them trend along a NWW to SEE direction and extend a distance of 750 km in this direction. These are two edifices nearby to the east of the plain, and these appear to be connected to another cluster of reflectors which extend along a SW to NE direction; similar to the Marte Vallis channel. Near the north and south boundaries of the western Cerberus plain, there are a small number of radar reflectors, and they drape deeper toward the boundaries, as indicated by the red arrows in Figures 3b and 3c. However, a different morphology is observed in the northern part of the Cerberus plain, south of Cerberus Fossae. There is a set of radar reflectors

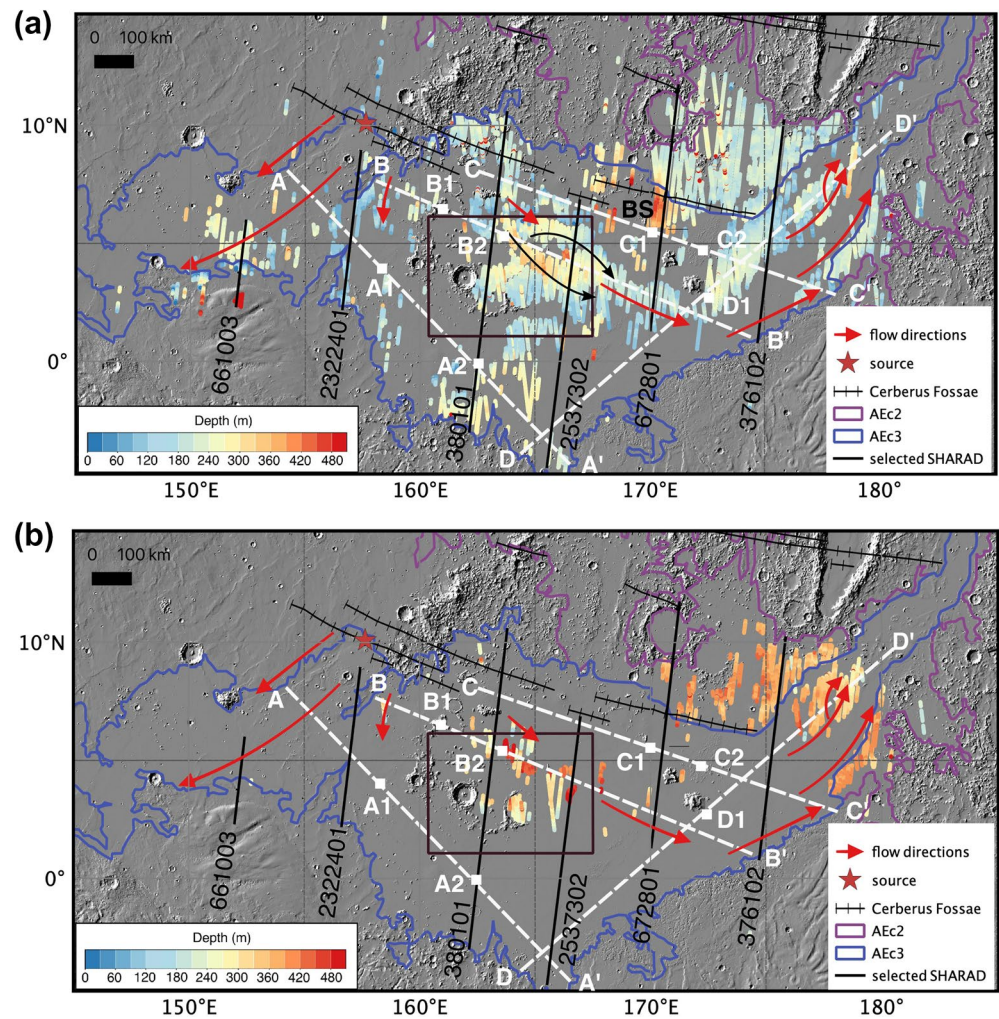


Figure 2. The first layer (a) and the second layer (b) of subsurface reflectors extracted from the SHARAD radargrams using manual digitization. The stars show the source of the outflow channel of Athabasca Valles and Grjotá Valles. Red lines with arrows are the postulated flow directions (Tanaka et al., 2014). The depth is derived by assuming a single dielectric constant of 3. The black straight lines that orient along NNE to SSW directions indicate the ground tracks of radargrams 661003, 2322401, 380101, 2537302, 672801, and 376102, which are also shown in Figure 3. White dashed lines are topographic profiles shown in Figure 4. The region in the red box is analyzed in detail in Figure 5. Black arrows indicate a possible channel and flow directions.

which are located deeper from the surface and appear like a bowl-like shape. This bowl-shaped feature extends ~290 km along the NW-SE direction and ~200 km along the SW-NE direction. The deepest radar reflectors that can be detected associated with this feature are located about 250 m below the surface. In the radargram from orbit 672801, the buried radar reflectors form a bowl shape, as shown in Figure 3e.

Apart from radargrams, topography in this region is also taken into consideration to infer flow directions and channel connections. Topography along the white dotted lines is plotted in Figure 4. As we can see, this plain has almost no elevation difference from north to south but has a slight tilted elevation from west to east. There is an elevation difference of about 400 m along AA', BB', and CC', which is oriented in a NW to SE direction. This is congruent with the spatial distribution of detected radar reflectors, indicating that the fluids probably flowed from NW to SE in the Cerberus plain. In addition, along profile of DD', we can see that D-D1 forms a channel-like shape which implies a flow direction from NW to SE. However, the

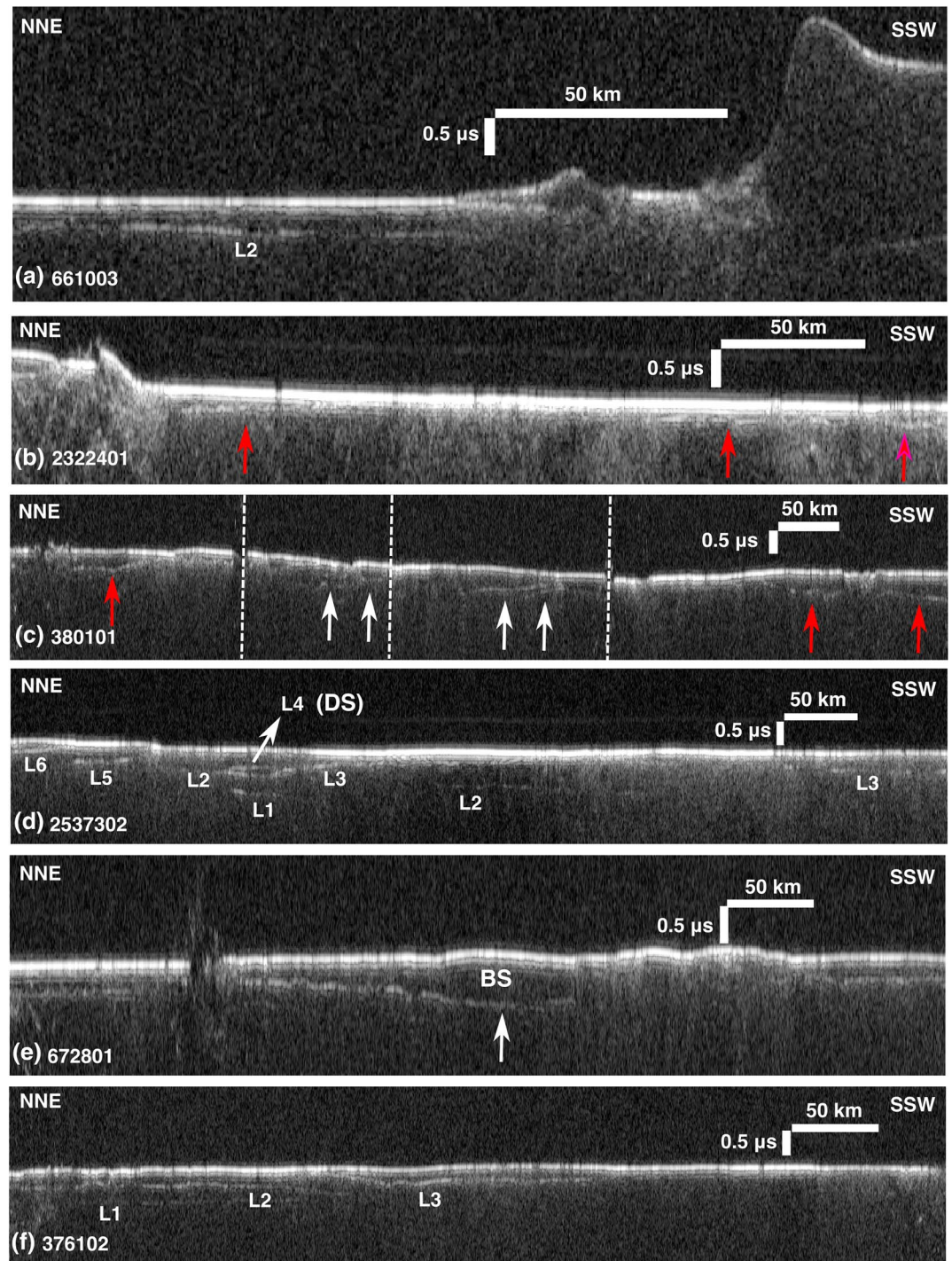


Figure 3. Radargrams (a) 661003, (b) 2322401, (c) 380101, (d) 2537302, (e) 672801, and (f) 376102. L1–L6 are layers found in central Cerberus plain. White arrows indicate layers which are noteworthy. Red arrows indicate the draped layers toward the northern and southern edges of Cerberus plain.

elevation starts to decrease from D1 to D', which corresponds to the locations where the L3 layer is detected near the source of Marte Vallis.

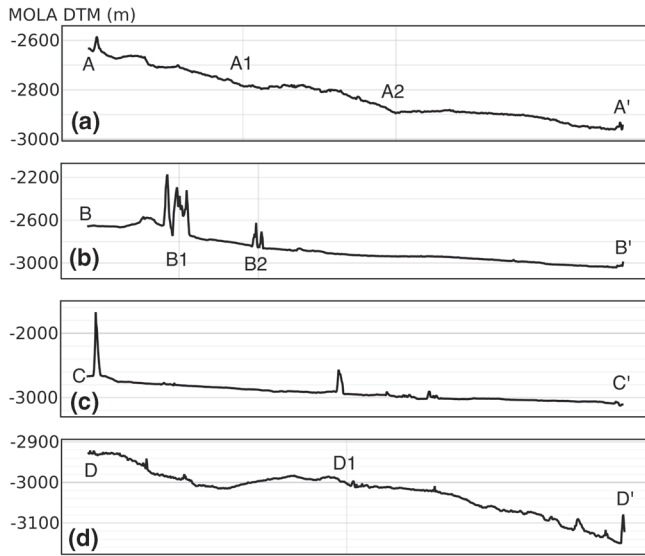


Figure 4. Topography extracted from MOLA DTM along four profiles: (a) AA', (b) BB', (c) CC', and (d) DD'. Their ground footprints are shown in Figure 2.

3.2. Infilled and Terraced Craters

In central Cerberus plain, there are two infilled craters which we label as CR1 and CR2, as seen in Figure 5a. Two interfaces can be observed in radargrams crossing CR1 (Figures 5c and 5d) and in radargrams crossing CR2 (Figures 5e and 5f). The range samples of the upper and lower layers from the surface reflector, are measured as $N_1 = 15.66 \pm 2.22$ and $N_2 = 25.36 \pm 3.27$, respectively. North of the eastern most infilled crater, there is one HiRISE image (ESP_044514_1840) depicting one small terraced crater (164.26°E, 3.95°N) which is labeled as T in Figure 5b. The average diameter and average depth are measured as about 1,200 m and about 229 m respectively. Two exposed layers can be observed in the northwest wall of this terraced crater. The along-track sampling distance of the SHARAD data is about 460 m; thus, it is too coarse to resolve this small crater. Two deeper layers are observed north of the terraced crater. Range samples of these two deeper layers are measured as $N_3 = 31.47 \pm 2.41$ and $N_4 = 47.77 \pm 2.94$, respectively. Therefore, three to four layers can be observed surrounding the CR2. The measurements are shown in Figure S2.

First, we attempt to estimate the dielectric constants by assuming that the two subsurface layers within the CR2 correspond to the two exposed layers of the terraced crater. The layer depths of the exposed layers can be measured using topographic data, such as CTX DTM or HiRISE DTM.

Figure 6 shows a triplet of HRSC, CTX and HiRISE synthesized images covering the terraced crater. These images are produced by overlaying using transparency grayscale ORIs (OrthoRectified Images) on the corresponding colorized and hill-shaded DTMs. Two exposed layers in the terraced crater can be identified both in the HiRISE and CTX imagery, which show a near perfect circular crater. However, the crater morphology in the HRSC DTM is ambiguous and terraces cannot be clearly discerned due to shadowing. Therefore, the following analyses is mainly based on CTX and HiRISE data.

Figure 7a shows an illustration of the profiles of the terraced crater. In order to measure the depth of the terraced layers, we identified the bench boundary of the upper and lower layers (indicated by TL₁ and TL₂, respectively) and measured their elevations, H_1 , H_2 , which were then compared with elevations of the pre-impact surface, H_s , to derive layer depths. Since the exposed layers can only be discerned in the northwest side as seen in Figure 7b, 13 radial lines from the crater center are selected, along which the intersection of the bench boundaries of exposed layers annotated by dots. Elevations of these dots are measured in both the HiRISE and CTX DTMs, and their measured values are listed in Table 1. From these measurements, the average depths of the upper and lower layer can be calculated as 123 ± 13 and 190 ± 9 m respectively when using HiRISE DTM. These values are 118 ± 12 and 189 ± 8 m when using CTX DTM. As we can see in Figure 7c, the HiRISE and CTX DTMs are well co-registered and consequently are consistent with each other; therefore, we averaged the layer depths between these two measurements, leading to upper and lower depths of $d_1 = 120.5 \pm 8.8$ m and $d_2 = 189.5 \pm 6.0$ m.

If the one-way time delay of one range sample in a radargram is Δt , then the vertical sampling distance can be expressed as $R = c\Delta t$, where c is the speed of light and the two-way time delay is 37.5 ns for SHARAD, leading to a value of $R = 5.625$ m. With a filling material of dielectric constant, ϵ , the depth of one layer can be calculated by its pixels numbers from the surface, N , as $d = c\Delta tN / \sqrt{\epsilon} = RN / \sqrt{\epsilon}$. Therefore, if we hypothesize that the two exposed layers in the wall of the terraced crater correspond to the two buried SHARAD layers, the dielectric constant of the material between surface and the first layer, ϵ_1 , can be estimated using Equation 1.

$$\sqrt{\epsilon_1} = \frac{RN_1}{d_1} \quad (1)$$

According to this equation, the dielectric constant of the first layer can be estimated to be about 0.53 ± 0.08 . This is estimated to be 1.40 ± 0.21 when replacing N_1 with N_2 . Both of these values are too low to be any

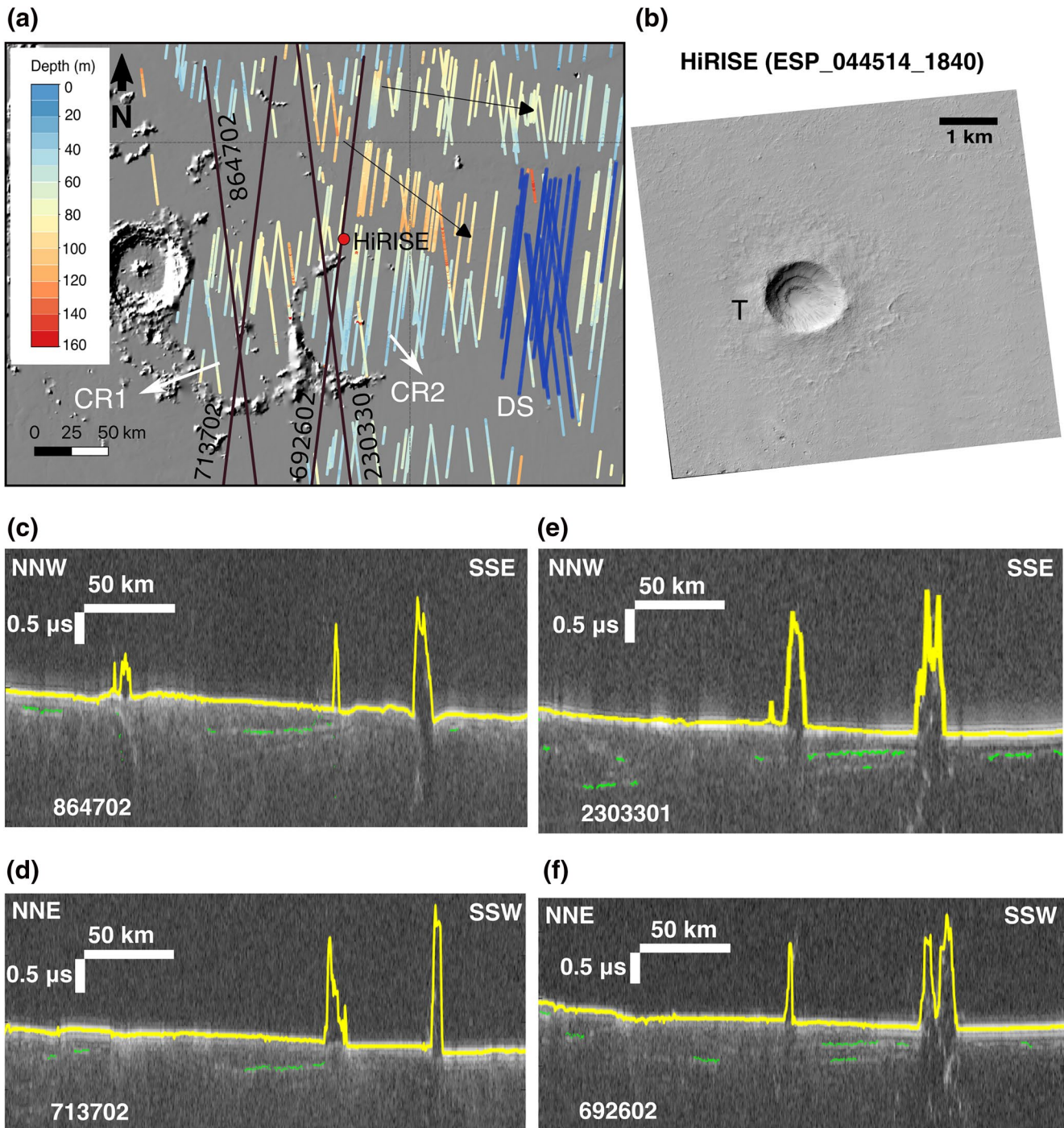


Figure 5. (a) A region of interest in the central Cerberus plain. Black arrows indicate the possible channel and flow directions. The red dot indicates the location of one terraced crater, which is imaged in (b) one HiRISE image (ESP_044514_1840). (c) and (e) are two radargrams (product IDs. 713702 and 864702) crossing one buried crater. (d) and (f) are two radargrams (product IDs. 2303301 and 692602) showing two layers of radar reflectors buried in one larger crater near the terraced crater. The yellow lines are the surfaces of the radargrams that are congruent with the MOLA DTM, and the green dots are automatically detected radar reflectors. The blue lines in (a) show the distribution of orbits where the subsurface streamlined island is identified in the radargrams.

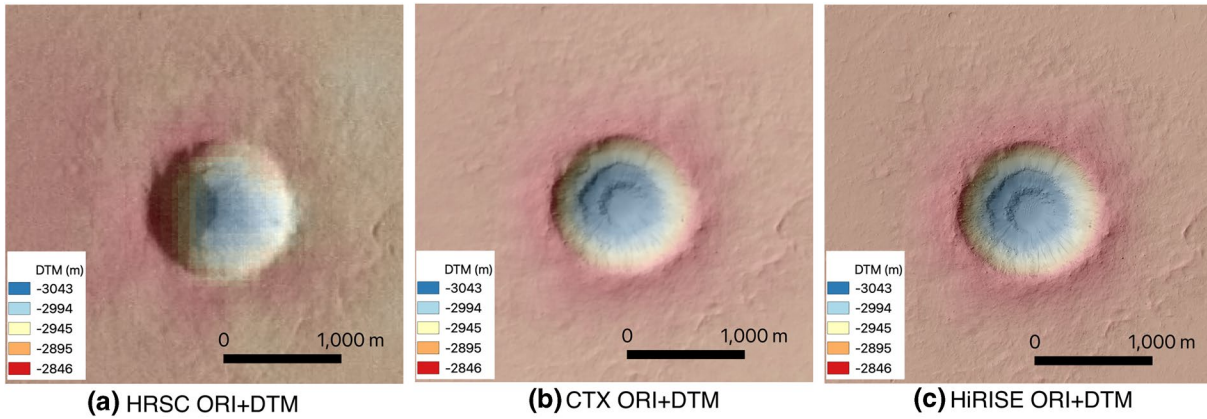


Figure 6. (a) HRSC ORI overlaid using transparency on a hill-shaded and colored by height HRSC DTM; (b) CTX ORI overlaid on a similarly visualized CTX DTM; and (c) HiRISE ORI overlaid on a similarly visualized on HiRISE DTM.

known geological material, which does not agree with the hypothesis that the two subsurface layers within the CR2 correspond to the two terraces of crater, T.

Excluding the two obvious layers within the CR2, we consider subsurface layers which are observed north of the CR2 and nearer to the terraced crater. Then the N_1 in the Equation 1 is replaced with N_3 , and the ϵ_1 can be calculated as 2.16 ± 0.32 . This is reasonable for geologic material and is slightly underestimated because the terraced crater is nearer the deeper end of the N_3 layer while we are using average values here. If we use $+3\sigma$ as the N_3 is dipping toward the terraced crater, the dielectric constant, ϵ_1 , is calculated as 3.12.

This estimation leads to an interpretation of mixture of water ice and dust between this layer and the surface. Since both the N_3 and N_4 layers are dipping southwards and there is no clear N_4 layers observed near the terraced crater, we cannot interpret the lower N_4 layer.

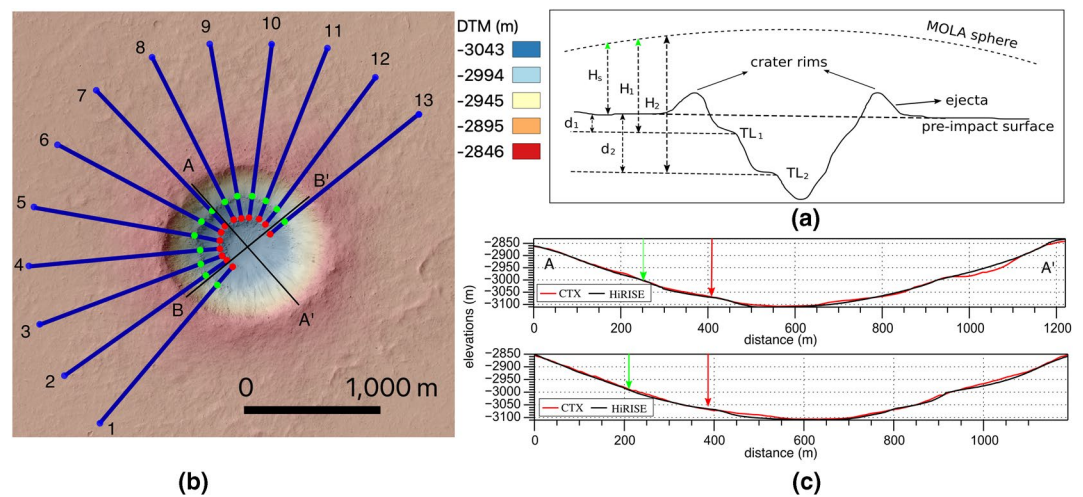


Figure 7. (a) Measurement of exposed layers on the HiRISE image and corresponding measurements of layer depths on CTX DTM. The red and green dots are selected along the blue lines which intersect the exposed layers. The blue dots are outside the crater ejecta for measuring pre-impact surface elevations. Elevations of blue, green, and red dots correspond to H_0 , H_1 , and H_2 shown in (b) profiling illustration of the terraced crater. Measurements of these elevations are listed in Table 1; (c) topography along profile AA' and BB', the green and red arrows indicate bench boundaries of the terraced layers.

Table 1
Measurements of Exposed Layer Depths in HiRISE and CTX DTMs

No.	HiRISE DTM (units: m)					CTX DTM (units: m)					
	H_s	H_1	H_2	d_1	d_2	H_s	H_1	H_2	d_1	d_2	
1	-2,881	-2,988	-3,064	107	183	-2,881	-2,993	-3,063	112	182	
2	-2,878	-3,005	-3,074	127	196	-2,879	-3,000	-3,072	121	193	
3	-2,881	-3,018	-3,080	137	199	-2,884	-3,015	-3,078	131	194	
4	-2,881	-3,029	-3,075	148	194	-2,882	-3,023	-3,074	141	192	
5	-2,880	-2,991	-3,081	111	201	-2,882	-2,998	-3,078	116	196	
6	-2,880	-3,014	-3,080	134	200	-2,880	-3,010	-3,079	130	199	
7	-2,878	-3,018	-3,074	140	196	-2,881	-3,010	-3,070	129	189	
8	-2,881	-3,009	-3,076	128	195	-2,878	-3,001	-3,081	123	203	
9	-2,881	-2,991	-3,065	110	184	-2,882	-2,995	-3,069	113	187	
10	-2,881	-2,995	-3,061	113	179	-2,883	-2,993	-3,064	110	181	
11	-2,883	-2,998	-3,067	115	184	-2,881	-2,984	-3,060	103	179	
12	-2,883	-3,000	-3,059	117	176	-2,879	-2,979	-3,060	100	181	
13	-2,884	-2,997	-3,065	113	181	-2,881	-2,989	-3,060	108	178	
Average value				123	190					118	189
Standard deviation				13	9					12	8

Note. The locations of measurements are shown in Figure 7.

3.3. Radar Stratigraphy of the Central Cerberus Plain

On analyzing the SHARAD profiles, one serendipitous discovery is the existence of one dome-like feature (DS) which sit on L2 as seen in Figure 3d. This dome-like feature is observed in 19 SHARAD radargrams whose product IDs are listed in Table S2 in the supporting information. Their transects are shown as blue lines in Figure 5a. We postulate that these 19 radargrams represent different profiles of the same buried feature. Figure 8 shows three examples of radargrams from NNE-SSW, whose product IDs are 736101, 879801, and 2537302. This feature is traced in the radargrams along 32 km for their shortest distance and 104 km for its longest distance. The average depths for these three layers are ~63, ~73, and ~138 m, respectively, assuming a single dielectric constant of 3.14.

In Figure 8, six layers are annotated as L1–L6, according to which we infer the sequence of their formation as six depositional and erosional episodes as shown in Figure 9. First, there may be a layer L1 deposited on the basal rock, which was covered by another layer L2 which was later eroded to form the surface of L2. Later, falling material or depositional material set at one side of the dome-like feature, formed the above mentioned dome-like feature observed in the radargrams. Finally, a veneer of material covered all this region, forming a flat-plain and surface of the preceding layers L3 at the edge of this region. The absence of any complex layering setting in other parts of Cerberus plain may be explained by channels carved by a single erosional period and later filled in by flood material.

Radar reflector boundaries belonging to this feature are converted to a 3D visualization as shown in Figure 10. The manually delineated results (in ASCII format) and a corresponding MATLAB script for their visualization are provided in the supporting information. The red point cloud forms a dome-shaped feature sitting on the base layer, which is elevated in the south and denoted by a green point cloud in Figures 10a and 10b. The layer colored in green appears like a depositional layer which makes the dome-shape feature above it less likely to be a streamlined island, while more likely to be talus from a previous deposit.

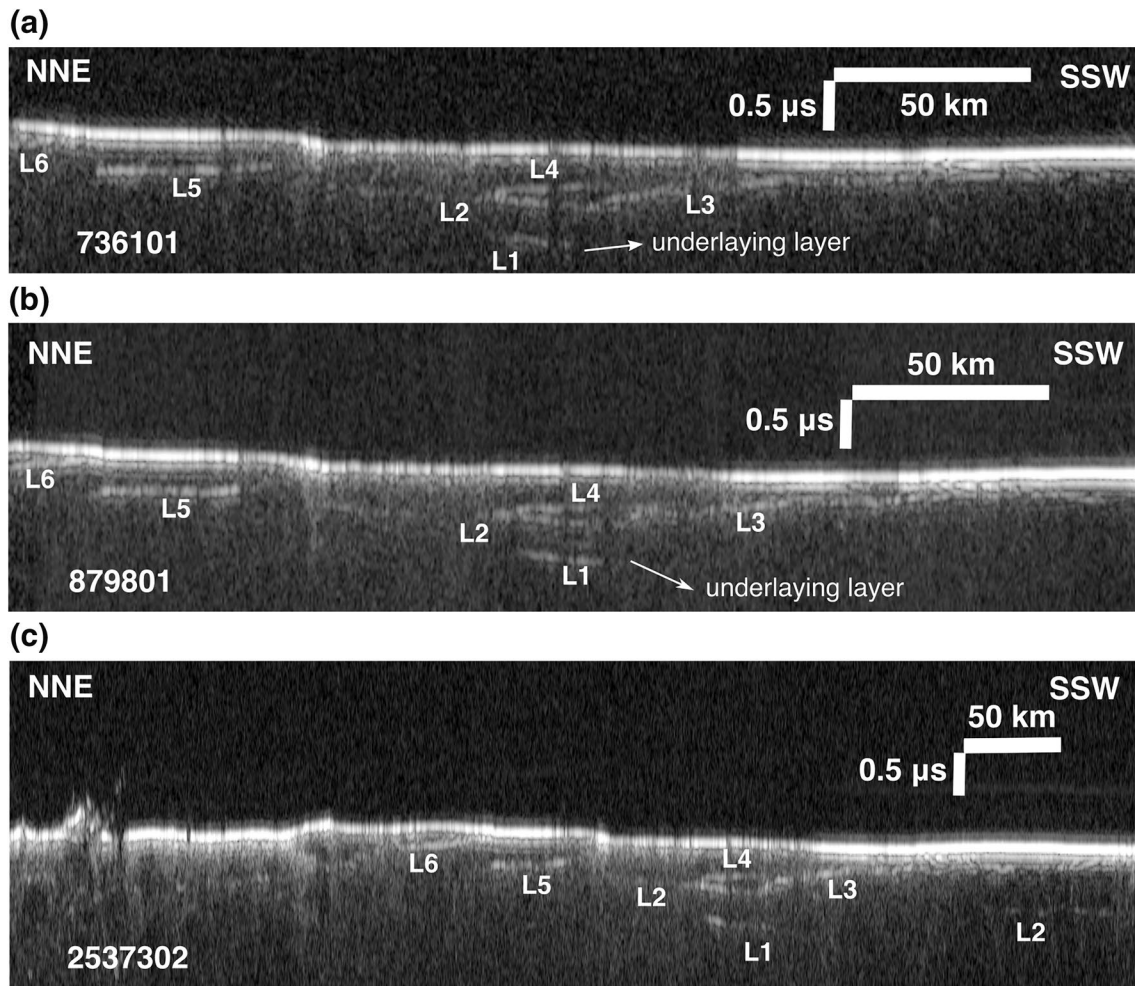


Figure 8. Radargrams of (a) 736101, (b) 879801, and (c) 2537302. L1–L6 are layers found in the central Cerberus plain.

4. Discussion

Previous studies have presented that only one layer of radar reflectors can be observed in a region of Athabasca basin, while in central Cerberus plain, seven layers are revealed (Morgan et al., 2015) and in Marte Vallis, three sets of radar reflectors (L1R, L2R, and R3) are observed (Morgan et al., 2013). In this study, a relationship between a number of layers and differences in the surficial geological units is inferred. The AEC₃ unit occupies Athabasca Valles and the channel of Marte Vallis where only one single layer can be observed below the surface. However, in Rahway Valles and central Cerberus plain, more than one layer can be observed, though in Rahway Valles, there appear to be two parallel layers while in central Cerberus plain, six layers are observed showing more complex morphology. The AEC₂ unit occupies most of the Rahway Valles and the central Cerberus plain features a high density of craters which indicate remnants of older units. In addition, considering the topography of Cerberus plain, we postulate that there may have been fluid flow from Athabasca Valles into the Cerberus plain, which is supported by Balme et al. (2010)'s study that the Athabasca basin is an almost closed basin, drained by two spillways, one of which is the Lethe Vallis in the southwest. Therefore, Lethe Vallis may be connected between Athabasca Valles and Cerberus plain. The fluids were either deposited in this plain or flowed further into Marte Vallis. The latter situation might be contradicted by the theory that the source of Marte Vallis is part of Cerberus Fossae, which is currently buried underground. Therefore, the former explanation is preferred. We postulate that the fluids were following from three possible channels indicated as AA', BB', CC' in Figure 4. The deep buried radar reflectors

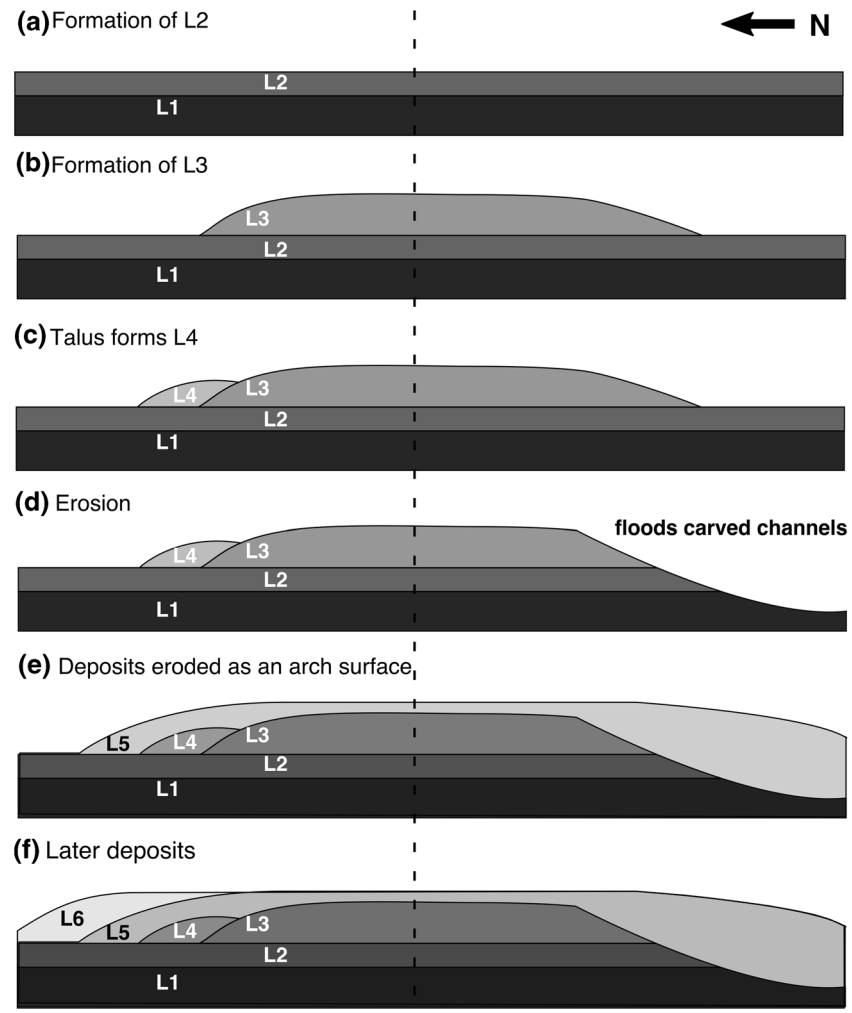


Figure 9. Schematic illustration of radar stratigraphy showing alternating depositional and erosional episodes in the study area. (a-f) are inferred six depositional and erosional episodes.

in the northern and central Cerberus plain which are annotated by BS in Figure 2 form bowl-shape features, which could be a reservoir of the fluids.

A terraced crater is identified in the Cerberus plain and depths of two terraces are measured. Near the terraced crater, three to four subsurface layers are observed in SHARAD radargrams. Two of them are observed within a large crater and the other two are observed north of the large crater, nearer to the terraced crater, which appear to correspond to these two terraces. These two deeper layers appear to correspond to L1 and L2 in Figure 9. We tried to constrain the dielectric constant of material covering the central Cerberus plain by using depths of these exposed layers that are measured in the HiRISE and CTX DTMs. Depths of the upper and lower exposed layers are measured as 120.5 and 189.5 m, and the upper one is matched with one subsurface layer outside the CR2, leading to dielectric constant estimations of 3.12 for the upper medium. This favors an interpretation that the surface material filling the surface and the detected radar reflectors is more likely to contain water ice or its composites with dry low-density materials (Watters et al., 2007).

Vaucher et al. (2009) analyzed the geologic contact and the volcanic history over the Cerberus plain, where they applied an average relationship between rim heights and diameters for fresh impact craters on Mars (Garvin et al. 2003) and a minimum curvature algorithm (Franke, 1982) to derive the depth of the substratum up to 350 m. The lowest layer detected by SHARAD of the dome-like feature is located ~138 m below surface when using a dielectric constant of 3.14. This indicates that SHARAD does not yet reach the substratum of most craters, especially large ones, which were formed before cratering started in the CEP region.

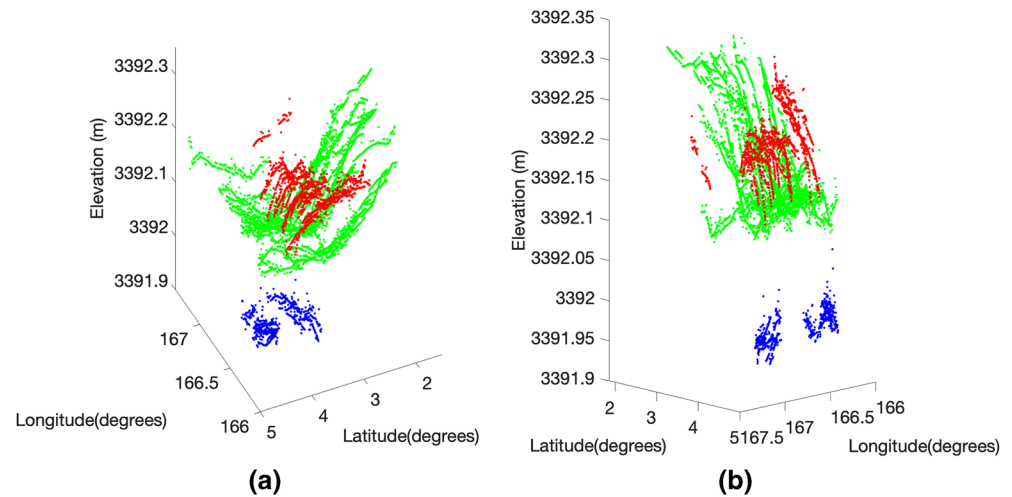


Figure 10. 3D visualization of the 3D digitized point clouds derived from the SHARAD radar profiles of the dome-like feature shown from two aspects. The subfigures of (a) and (b) are presented for viewing angles from the northwest and northeast.

Through analysis of the complex layering structure in the central Cerberus plain, we propose a model of depositional and erosional processes which occur in this area. This model indicates six layers formed during alternating depositional and erosional episodes. In other areas, fewer layers of subsurface radar reflectors are observed. This unique dense layering in this region may be attributed to dense cratering in this region, which might protect depositional layers from erosion by flooding. Erosion may be more intense in other parts where fewer layers of subsurface radar reflectors are observed. It is in these locations that ancient aqueous floods might have carved out the channels that connect Athabasca Valles, Marte Vallis to Cerberus plain. These channels may be covered by later lava flows as proposed in previous studies (Morgan et al., 2013).

5. Conclusions

In this study, we investigated subsurface radar reflectors observed in SHARAD data over the central Elysium Planitia region. A new automated method was demonstrated to process SHARAD data to obtain distribution and depth maps of multiple layers of subsurface reflection. Manual digitization was also used to validate the automated derived results. From the resulting depth maps of the radar reflectors, connections between the Cerberus plain and Athabasca Valles and Marte Vallis is inferred. Ancient fluid flows may have taken place from Athabasca Valles into the Cerberus plain, and then either have been deposited in the low reservoirs in the Cerberus plain or have flowed further into Marte Vallis. Topographic analysis suggests three possible channels in this region. In the central region of the Cerberus plain, exposed layers are found on the rim of a terraced crater. Matching the exposed layers of the terraced crater with the detected subsurface layers north of the southern infilling crater, the dielectric constants of the media between the uppermost layer and the surface can be estimated to be 3.12. This estimation supports an interpretation that this region contains shallow buried water ice though dry low-density materials cannot be excluded (Watters et al., 2007).

In the central Cerberus plain, a dome-like feature is indicated in SHARAD signals which may reach the pre-impacted surface in this region. In addition, a stratigraphic analysis associated with this region indicates that six layers are present, revealing a complex depositional and erosional history in this region. The differences between this region and other parts of the Cerberus plain may be explained by dense craters in this region, which might protect depositional layers from erosion by flooding. Interpretation of the exposed deep layers of such a small terraced crater and construction of multi-layer modeling in Cerberus plain should be carried out in future work.

Author Contributions

S. Xiong processed and analyzed radar data, measured layer depths of the terraced crater on the DTMs and drafted the manuscript. Y. Tao produced a CTX DTM (F22_044514_1831_XN_03N195 W and G02_018853_1837_XN_03N195 W) and a HiRISE DTM (ESP_043815_1840 and ESP_044514_1840), and reviewed the manuscript for technical issues. D. M. Persaud proposed the terraced crater in the HiRISE image, produced an initial CTX DTM (F21_043815_1833_XN_03N195 W and G02_018853_1837_XN_03N195 W) and reviewed the manuscript in terms of geologic description. J. D. Campbell assisted in analysis of CRISM (Compact reconnaissance imaging spectrometer for Mars) data, though not included finally and reviewed the manuscript and revised it in geological terms. A. R. D. Putri assisted in the analysis of CTX imagery though not included finally and reviewed the manuscript and provided technical advice. Prof. J.-P. Muller proposed the study of the CEP, analyzed the data and reviewed the manuscript.

Data Availability Statement

SHARAD data used in this study are released by SHARAD Science Team, U.S. and are available from the Planetary Data System (PDS) Geosciences Node of Washington University at St. Louis, USA (WUSTL-PDS) (https://pds-geosciences.wustl.edu/mro/mro-m-sharad-5-radargram-v1/mrosh_2001/). The HiRISE imagery is available from data repository at the University of Arizona (https://www.uahirise.org/ESP_044514_1840). NASA's Jet Propulsion Laboratory, a division of the California Institute of Technology in Pasadena, Calif., manages the Mars Reconnaissance Orbiter for NASA's Science Mission Directorate, Washington. The HiRISE camera was built by Ball Aerospace and Technology Corporation and is operated by the University of Arizona. The orthorectified CTX imagery and derived DTM can be searched at iMars website (<http://www.i-mars.eu/publications/products/>) and thence to the ESA-PSA Guest Storage Facility (https://www.cosmos.esa.int/web/psa/ucl-mssl-mars-cep_ctx-hirise_v1.0). The output products are available from the ESA Guest Storage Facility (The DOI for the CTX DTM collection is 10.5270/esa-lqefjdl). This facility is described in Muller et al. (2019).

Acknowledgments

The authors would like to thank the China Scholarship Council and University College London for providing a scholarship from the Dean of MAPS prize to the first author and the European Commission for providing travel support from the European Union's Seventh Framework Program (FP7/20072013) under iMars grant agreement no 607379 and partial funding from the STFC "MSSL Consolidated Grant" ST/K000977/1. The authors would like to thank the SHARAD team at the NASA Jet Propulsion Laboratory (JPL), USA, for providing SHARAD data, and to express their gratitude to Dr. Susan Conway for commenting on the first draft of the paper. The authors would like to thank the UK Space Agency for support for the DTM production from Aurora award reference number ST/S001891/1.

References

- Alberti, G., Castaldo, L., Orseoi, R., Frigeri, A., & Cirillo, G. (2012). Permittivity estimation over Mars by using SHARAD data: The Cerberus Palus area. *Journal of Geophysical Research: Planets*, 117(E9), E09008. <https://doi.org/10.1029/2012JE004047>
- Balme, M. R., Gallagher, C. J., Page, D. P., Murray, J. B., Muller, J. P., & Kim, J. R. (2010). The Western Elysium Planitia Paleolake. In N. A. Cabrol & E. A. Grin (Eds.), *Lakes on Mars* (pp. 275–301). The Netherlands: Elsevier.
- Berman, D. C., & Hartmann, W. K. (2002). Recent fluvial, volcanic, and tectonic activity on the Cerberus plains of Mars. *Icarus*, 159(1), 1–17. <https://doi.org/10.1006/icar.2002.6920>
- Bramson, A. M., Byrne, S., Putzig, N. E., Sutton, S., Plaut, J. F., Charles Brothers, T., & Holt, J. W. (2015). Widespread Excess Ice in Arcadia Planitia, Mars. *Geophysical Research Letters*, 42(16), 6566–6574. <https://doi.org/10.1002/2015GL064844>
- Burr, D. M., Carling, P. A., Beyer, R. A., & Lancaster, N. (2004). Flood-formed dunes in Athabasca Valles, Mars: morphology, modeling, and implications. *Icarus*, 171(1), 68–83. <https://doi.org/10.1016/j.icarus.2004.04.013>
- Burr, D. M., Grier, J. A., McEwen, A. S., & Keszthelyi, L. P. (2002). Repeated aqueous flooding from the Cerberus Fossae: Evidence for very recently extant, deep groundwater on Mars. *Icarus*, 159(1), 53–73.
- Campbell, B. A., & Morgan, G. A. (2018). Fine-scale layering of Mars polar deposits and signatures of ice content in nonpolar material from multiband SHARAD data processing. *Geophysical Research Letters*, 45, 1759–1766. <https://doi.org/10.1002/2017GL075844>
- Carr, M. H. (1996). *Water on Mars*. New York, NY: Oxford University Press, pp. 1–248.
- Cassanelli, J. P., & Head, J. W. (2018). Formation of outflow channels on Mars: Testing the origin of Reull Vallis in Hesperia Planum by large-scale lava-ice interactions and top-down melting. *Icarus*, 305, 56–79. <https://doi.org/10.1016/j.icarus.2018.01.001>
- Clifford, S. M. (1993). A model for the hydrologic and climate behavior of water on Mars. *Journal of Geophysical Research: Planets*, 98, 10973–11016. <https://doi.org/10.1029/93JE00225>
- Durrant, L., Balme, M. R., Carling, P. A., & Grindrod, P. M. (2017). Aqueous dune-like bedforms in Athabasca Valles and neighboring locations utilized in palaeoflood reconstruction. *Planetary and Space Science*, 148, 45–55. <https://doi.org/10.1016/j.pss.2017.10.008>
- Franke, R. (1982). Smooth interpolation of scattered data by local thin plate splines. *Computers and Mathematics With Applications*, 8(4), 273–281.
- Garvin, J. B., Sakimoto, S. E. H., & Frawley, J. J. (2003). *Craters on Mars: Global geometric properties from gridded MOLA topography*. Sixth International Conference on Mars, Lunar and Planetary Science and Exploration, Washington DC., United States, Sep. 09, 2003.
- Harrison, K. P., & Grimm, R. E. (2005). Groundwater-controlled valley networks and the decline of surface runoff on early Mars. *Journal of Geophysical Research-Planets*, 110(E12S16), 1–17. <https://doi.org/10.1029/2005JE002455>
- Head, J. W., & Marchant, D. R. (2003). Cold-based mountain glaciers on Mars: Western Arsia Mons. *Geology*, 31, 641–644. [https://doi.org/10.1130/0091-7613\(2003\)031<0641:CMGOMW>2.0.CO;2](https://doi.org/10.1130/0091-7613(2003)031<0641:CMGOMW>2.0.CO;2)
- Jaeger, W. L., Keszthelyi, L. P., McEwen, A. S., Dundas, C. M., & Russell, P. S. (2007). Athabasca Valles, Mars: a lava-draped channel system. *Science*, 317, 1709–1711. <https://doi.org/10.1126/science.1143315>
- Jaeger, W. L., Keszthelyi, L. P., McEwen, A. S., Titus, T. N., Dundas, C. M., & Russell, P. S. (2008). Response to comment on "Athabasca Valles, Mars: A lava-draped channel system". *Science*, 320, 1588. <https://doi.org/10.1126/science.1155124>

- Jaeger W. L., Keszthelyi L. P., Skinner J. A., Milazzo M. P., McEwen A. S., Titus T. N., et al. (2010). Emplacement of the youngest flood lava on Mars: A short, turbulent story. *Icarus*, *205*(1), 230–243. <http://dx.doi.org/10.1016/j.icarus.2009.09.011>
- Keszthelyi, L., Jaeger, W. L., & Dundas, C. M. (2017). Investigating the role of water and lava in Athabasca Valles, Mars. Lunar and Planetary Science Conference (Vol. 48), March 20–24, 2017, The Woodlands, Texas.
- Kossacki, K. J., Markiewicz, W. J., Smith, M. D., Page, D., & Murray, J. (2006). Possible remnants of a frozen mud lake in southern Elysium, Mars. *Icarus*, *181*(2), 363–374. <https://doi.org/10.1016/j.icarus.2005.11.018>
- Lanagan, P. D. (2004). Geologic history of the Cerberus Plains, Mars. PhD thesis, University of Arizona, Arizona, U.S.
- Malin, M. C., Bell, J. F., Cantor, B. A., Caplinger, M. A., Calvin, W. M., Clancy, R. T., et al. (2007). Context camera investigation on board the Mars reconnaissance orbiter. *Journal of Geophysical Research: Planets*, *112*(E5), 1–25. <https://doi.org/10.1029/2006JE002808>
- Malin, M. C., Edgett, K. S., Cantor, B. A., Caplinger, M. A., Danielson, E., Jensen, E. H., et al. (2010). An overview of the 1985–2006 Mars Orbiter Camera Science Investigation. *Mars, The International Journal of Mars Science and Exploration*, *5*, 1–60. <https://doi.org/10.1555/mars.2010.0001>
- McEwen, A., Eliason, E., Bergstrom, J., Bridges, N., Hansen, C., Delamere, W., et al. (2007). Mars reconnaissance orbiter's high resolution imaging science experiment (HiRISE). *Journal of Geophysical Research: Planets*, *112*(E05S02), 1–40. <https://doi.org/10.1029/2005JE002605>
- Morgan, G. A., Campbell, B. A., Carter, L. M., & Plaut, J. J. (2015). Evidence for the episodic erosion of the Medusae Fossae Formation preserved within the youngest volcanic province on Mars. *Geophysical Research Letters*, *42*, 7336–7342. <https://doi.org/10.1002/2015GL065017>
- Morgan, G. A., Campbell, B. A., Carter, L. M., Plaut, J. J., & Phillips, R. J. (2013). 3D reconstruction of the source and scale of buried young flood channels on Mars. *Science*, *340*(6132), 607–610. <https://doi.org/10.1126/science.1234787>
- Muller, J. P., Tao, Y., Putri, A. R. D., Watson, G., Beyer, R., Alexandrov, O., et al. (2019). 3D Imaging tools and geospatial services from joint European-USA collaborations. *European Planetary Science Conference*, *13*, EPSC-DPS2019–1355–2.
- Murray, J. B., Muller, J. P., Neukum, G., Werner, S. C., van Gasselt, S., Hauber, E., et al. (2005). Evidence from the Mars Express High Resolution Stereo Camera for a frozen sea close to Mars' equator. *Nature*, *434*(7031), 352–356. <https://doi.org/10.1038/nature03379>
- Orosei, R., Cartacci, M., Cicchetti, A., Noschese, R., Federico, C., Frigeri, A., et al. (2007). Radar subsurface sounding over the putative frozen sea in Cerberus Palus, Mars. AGU Fall Meeting Abstracts, pp. 1–4. <https://doi.org/10.1109/ICGPR.2010.5550143>
- Plescia, J. B. (1990). Recent flood lavas in the Elysium region of Mars. *Icarus*, *88*(2), 465–490. [https://doi.org/10.1016/0019-1035\(90\)90095-Q](https://doi.org/10.1016/0019-1035(90)90095-Q)
- Plescia, J. B. (2003). Cerberus Fossae, Elysium, Mars: A source for lava and water. *Icarus*, *164*(1), 79–95. [https://doi.org/10.1016/S0019-1035\(03\)00139-8](https://doi.org/10.1016/S0019-1035(03)00139-8)
- Ramsdale, J. D., Balme, M. R., Conway, S. J., & Gallagher, C. (2015). Ponding, draining and tilting of the Cerberus Plains; a cryolacustrine origin for the sinuous ridge and channel networks in Rahway Vallis, Mars. *Icarus*, *253*, 256–270. <https://doi.org/10.1016/j.icarus.2015.03.005>
- Seu, R., Biccari, D., Orosei, R., Lorenzoni, L. V., Phillips, R. J., Marinangeli, L., et al. (2004). SHARAD: The MRO 2005 shallow radar. *Planetary and Space Science*, *52*(1), 157–166. <https://doi.org/10.1016/j.pss.2003.08.024>
- Slavney, S., & Orosei, R. (2007). SHALLOW radar reduced data record software interface specification, Version 1.0. Retrieved from https://pds-geosciences.wustl.edu/mro/mro-m-sharad-4-rdr-v1/mrosh_1001/document/rdrsis.pdf
- Stuurman, C. M., Osinski, G. R., Holt, J. W., Levy, J. S., Brothers, T. C., Kerrigan, M., & Campbell, B. A. (2016). SHARAD detection and characterization of subsurface water ice deposits in Utopia Planitia, Mars. *Geophysical Research Letters*, *43*, 9484–9491. <https://doi.org/10.1002/2016GL070138>
- Tanaka, K. L., Skinner, J. A., Dohm, J. M., Irwin, R. P. III., Kolb, E. J., Fortezzo, C. M., et al. (2014). *Geologic map of Mars*, Scientific Investigations Map 3292, Reston, VA: U.S. Geological Survey. <https://doi.org/10.3133/sim3292>
- Tao, Y., Muller, J. P., Sidiropoulos, P., Xiong, S. T., Putri, A. R. D., Walter, S. H. G., et al. (2018). Massive Stereo-Based DTM Production for Mars on Cloud Computers. *Planetary and Space Science*, *154*, 30–58. <https://doi.org/10.1016/j.pss.2018.02.012>
- Vaucher, J., Baratoux, D., Toplis, M. J., Pinet, P., Mangold, N., & Kurita, K. (2009). The morphologies of volcanic landforms at Central Elysium Planitia: Evidence for recent and fluid lavas on Mars. *Icarus*, *200*(1), 39–51. <https://doi.org/10.1016/j.icarus.2008.11.005>
- Voigt, J. R., & Hamilton, C. W. (2018). Investigating the volcanic versus aqueous origin of the surficial deposits in Eastern Elysium Planitia, Mars. *Icarus*, *309*, 389–410. <https://doi.org/10.1016/j.icarus.2018.03.009>
- Watters, T. R., Campbell, B., Carter, L., Leuschen, C. J., Plaut, J. J., Picardi, G., et al. (2007). Radar sounding of the Medusae Fossae Formation Mars: Equatorial ice or dry, low-density deposits? *Science*, *318*(5853), 1125–1128. <https://doi.org/10.1126/science.1148112>
- Xiong, S., & Muller, J. P. (2019). Automated reconstruction of subsurfaces in Promethei Lingula over the Martian south pole by using SHARAD Data. *Planetary and Space Science*, *166*, 59–69. <https://doi.org/10.1016/j.pss.2018.08.001>

Erratum

In the originally published version, an acknowledgment had been omitted, and there was a mismatch of SHARAD productIDs between Figure 2 content and caption. The acknowledgments and Figure 2 have been updated, and this version may be considered the authoritative version of record.